Pageoph, Vol. 115 (1977), Birkhäuser Verlag, Basel

Barotropic-Baroclinic Instability of Mean Zonal Wind During Summer Monsoon

By J. SHUKLA[1])

Abstract – Barotropic-Baroclinic instability of horizontally and vertically shearing mean monsoon flow during July is investigated numerically by using a 10-layer quasi-geostrophic model. The most unstable mode has a wavelength of about 3000 km and westward phase speed of about 15 m sec^{-1}. The most dominant energy conversion is from zonal kinetic energy to eddy kinetic energy. The structure of the most unstable mode is such that the maximum amplitude is concentrated at about 150 mb and the amplitude at the lowest layers is negligibly small. Barotropic instability of the zonal flow at 150 mb seems to be the primary excitation mechanism for the most unstable mode which is also similar to the observed westward propagating waves in the upper troposphere during the monsoon season. The results further suggest that Barotropic-Baroclinic instability of the mean monsoon flow cannot explain the occurrence of monsoon depressions which have their maximum amplitude at the lower levels and are rarely detected at 200 mb.

Key words: Monsoon; Mean zonal wind; Barotropic-baroclinic instability.

1. Introduction

It is observed that during the northern summer an extensive low-pressure area persists between north Africa and east China, and its central area lies over west Pakistan, where the lowest mean surface pressure observed anywhere on the globe exists during June–September. The southeasterly trade winds of the southern hemisphere, which cross the equator under the influence of this thermal forcing due to asymmetric continentality, and turn into southwesterly currents, are referred to as the southwest monsoon. Although the monsoonal flow pattern over the Indian region persists for about four months, June through September, the mean conditions during July are considered to represent the most typical structure of the mean monsoon circulation. The vertical structure of the mean circulation is characterized by lower tropospheric westerlies and upper tropospheric easterlies, the transition occurs at about 500 mb. The mean circulation is also characterized by appreciable horizontal shear.

The purpose of this paper is to carry out the barotropic-baroclinic instability analysis of the horizontally and vertically shearing mean monsoon flow during July

[1]) Massachusetts Institute of Technology, Cambridge, Mass. 02139, USA.

along 85°E. The purpose of such linear stability analyses is to see if the dynamical structure of the observed mean flow is such that it permits growth of infinitesimal linear perturbations, and if it does, the flow is considered to be 'unstable'. If the necessary and sufficient conditions for instability are satisfied, it may provide an explanation for the occurrence of disturbances which are observed during the monsoon season. The plausibility of such explanation would, of course, depend upon the agreements between the most unstable mode and the observed disturbances, with respect to the wavelength, phase speed, structure and energetics.

Figure 1 shows the cross-section of mean monthly zonal wind speed for the month of July along 85°E from 20°S to 40°N. One of the noteworthy features of this cross-section is the presence of easterly winds between the two westerly maxima. Such a structure of the zonal flow is favorable for satisfying the necessary conditions for the internal jet instability (CHARNEY and STERN, 1962). KRISHNAMURTI *et al.* (1975) have shown that for the synoptic situation studied by them, the necessary condition for the joint barotropic-baroclinic instability was satisfied. However, the instability analysis of the horizontally and vertically shearing monsoon flow has not been carried out before. This paper gives the results of the instability analysis of the zonal flow along 85°E.

One of the necessary conditions for the joint barotropic-baroclinic instability is that the gradient of potential vorticity on an isentropic surface should vanish in the region. Figure 2 shows the cross section of potential vorticity along 85°E. It is seen that the necessary condition for instability is satisfied. Figure 3 shows similar

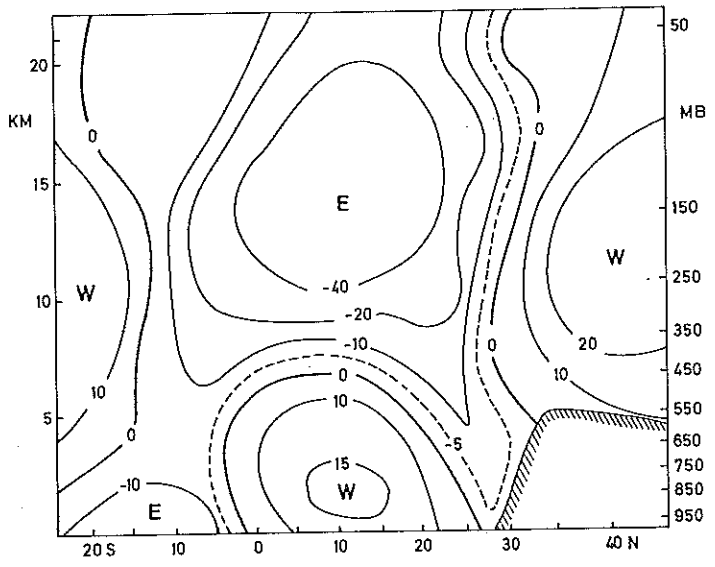

Figure 1
Cross-section along 85E for the observed mean July values of zonal wind (knots).

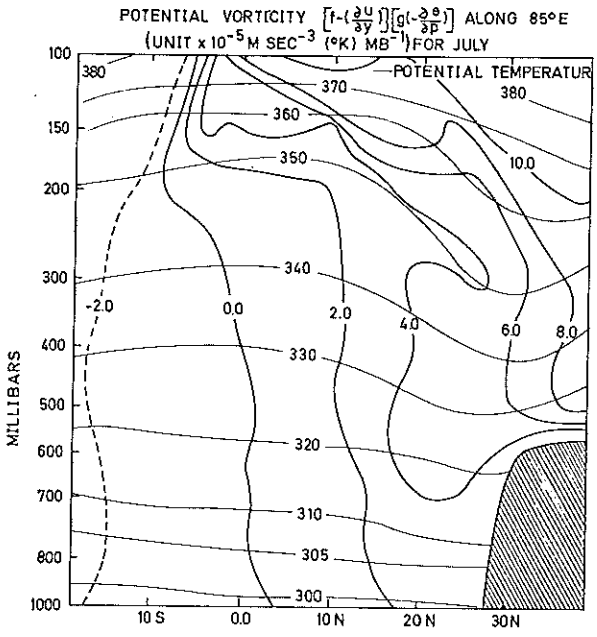

Figure 2
Cross-section of potential vorticity (10^{-5} ms^{-3} mb^{-1} (°K)) along 85E.

cross-sections along 73°E and 100°E. The necessary condition is satisfied in these cross sections also. Homogeneity of the potential vorticity field for a longitudinal span of about 30° (longitude) justifies a linear perturbation analysis in which large scale flow is assumed to be homogeneous along x (and perturbations are sinusoidal along x).

2. *The mathematical model*

The combined barotropic-baroclinic instability of mean monsoon zonal flow, $\overline{U}(y, p)$ is examined using a ten-layer quasi-geostrophic model. Because $\overline{U}$ is a function of y and p, the problem becomes non-separable, and this is a manifestation of the fact that there are two sources of energy (available kinetic energy and available potential energy).

Therefore, the initial value approach to instability analysis is used in which the linearized perturbation equations for a given wavelength are numerically integrated in time for an arbitrary initial condition. The integration is continued until the phase speeds and the growth rates converge to their constant values over the whole computational domain. These are the values of phase speed and growth rate for the most unstable mode. Integrations are performed for a range of wavelengths. The linearized

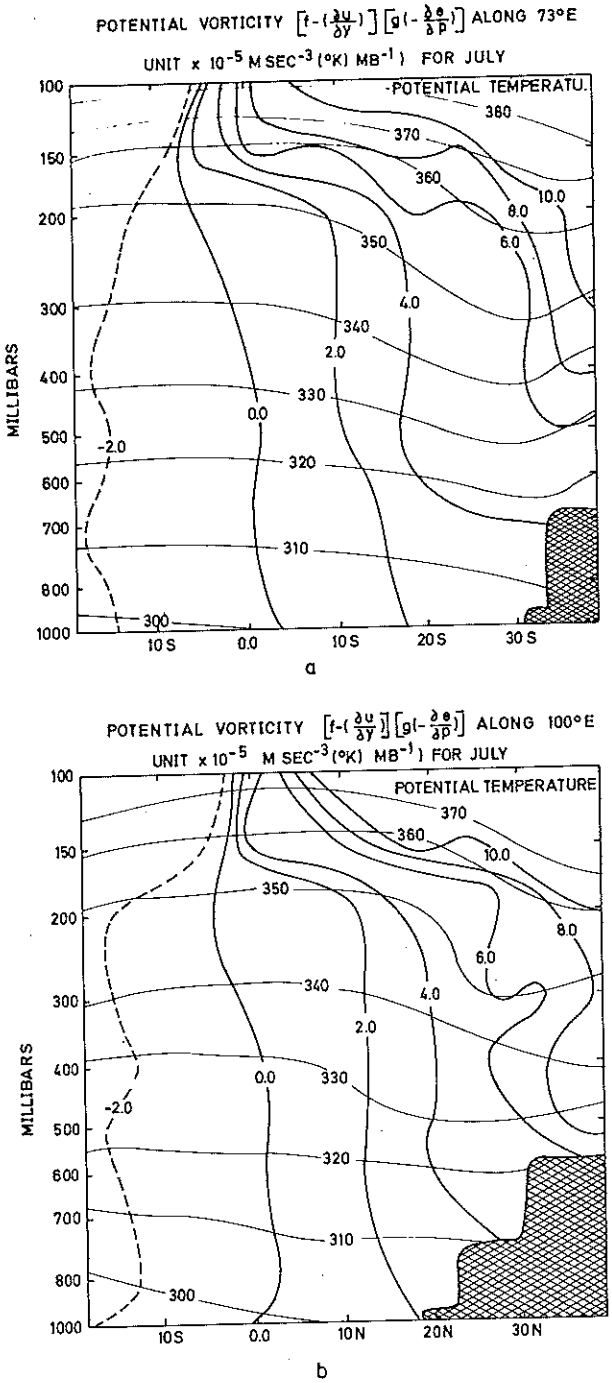

Figure 3
Cross-section of potential vorticity (10^{-5}ms^{-3} mb^{-1} (K°)) along (a) 73E, (b) 100E.

form of the vorticity and thermal equation may be written as:

$$\left(\frac{\partial}{\partial t} + \overline{U}\frac{\partial}{\partial x}\right)\nabla^2\psi' + \left(\beta - \frac{\partial^2\overline{U}}{\partial y^2}\right)\frac{\partial\psi'}{\partial x} - f_0\frac{\partial\omega'}{\partial p} = 0 \tag{2.1}$$

$$\left(\frac{\partial}{\partial t} + \overline{U}\frac{\partial}{\partial x}\right)\frac{\partial\psi'}{\partial p} - \frac{\partial\overline{U}}{\partial p}\frac{\partial\psi'}{\partial x} + \frac{\sigma\omega'}{f_0} = 0 \tag{2.2}$$

where ψ' and ω' are the perturbation stream function and vertical velocity (dp'/dt), respectively. σ is the stability parameter, which is a function of p only, and is given as:

$$\sigma(\bar{p}) = -\frac{R\overline{T}}{p\overline{\theta}}\frac{\partial\overline{\theta}}{\partial p} \tag{2.3}$$

where the bar ($\bar{}$) denotes the mean over an isobaric surface. f_0 is the constant value of the coriolis parameter and $\beta = \partial f/\partial y$. Assuming geostrophic balance between the mass field and the motion fields, we may derive the omega equation for ω' from (2.1) and (2.2), viz:

$$f_0\frac{\partial^2\omega'}{\partial p^2} + \frac{\sigma}{f_0}\nabla^2\omega' = \frac{\partial}{\partial p}\left\{(\overline{U}\nabla^2 + \beta - U_{yy})\frac{\partial\psi'}{\partial x}\right\} - \nabla^2\left\{\overline{U}\frac{\partial}{\partial p}\left(\frac{\partial\psi'}{\partial x}\right) - \frac{\partial\overline{U}}{\partial p}\frac{\partial\psi'}{\partial x}\right\}. \tag{2.4}$$

The first and second terms on the right-hand side of (2.4) are respectively the differential vorticity advection and the Laplacian of thickness advection. (A diagnostic ω equation yields that value of vertical velocity that is needed to maintain geostrophic and hydrostatic balance.)

The perturbation ψ' is taken to be of the form

$$\psi'(x, y, p, t) = \mathrm{Re}\{\Psi(y, p, t)\, e^{ikx}\}$$

where Ψ is complex. k is the wavenumber along x.

$$\Psi = \Psi_r + i\Psi_i$$

$$\Psi = \{F_r(y, p) + iF_i(y, p)\}\, e^{(\nu - ikc)t}.$$

Then,

$$\Psi_r = \{F_r\cos(kct) + F_i\sin(kct)\, e^{\nu t}$$

and

$$\Psi_i = \{F_i\cos(kct) - F_r\sin(kct)\}\, e^{\nu t}.$$

Solving for ν and c, we obtain the growth rate

$$\nu = \frac{\Psi_r(\partial\Psi_r/\partial t) + \Psi_i(\partial\Psi_i/\partial t)}{\Psi_r^2 + \Psi_i^2} \tag{2.5}$$

and the phase speed

$$c = \frac{\Psi_i(\partial\Psi_r/\partial t) - \Psi_r(\partial\Psi_i/\partial t)}{k(\Psi_r^2 + \Psi_i^2)}. \tag{2.6}$$

We may also write

$$w' = \mathrm{Re}\,\{W e^{ikx}\}$$

where

$$W = W_r + iW_i.$$

We may decompose (2.1) and (2.3) for the real and imaginary parts of the complex amplitudes Ψ and W.

Since

$$\nabla^2 = \left(-k^2 + \frac{\partial^2}{\partial y^2}\right)$$

we have

$$\frac{\partial}{\partial t}\left(-k^2 + \frac{\partial^2}{\partial y^2}\right)\Psi_r = \overline{U}k\left(-k^2 + \frac{\partial^2}{\partial y^2}\right)\Psi_i + (\beta - \overline{U}_{yy})k\Psi_i + f_0\frac{\partial W_r}{\partial p} \tag{2.7}$$

$$\frac{\partial}{\partial t}\left(-k^2 + \frac{\partial^2}{\partial y^2}\right)\Psi_i = -\overline{U}k\left(-k^2 + \frac{\partial^2}{\partial y^2}\right)\Psi_r - (\beta - \overline{U}_{yy})k\Psi_r + f_0\frac{\partial W_i}{\partial p} \tag{2.8}$$

$$\frac{\sigma}{f_0}\left(-k^2 + \frac{\partial^2}{\partial y^2}\right)W_r + f_0\frac{\partial^2 W_r}{\partial p^2} = \left[k\left(-k^2 + \frac{\partial^2}{\partial y^2}\right)\left\{\overline{U}\frac{\partial\Psi_i}{\partial p} - \Psi_i\frac{\partial\overline{U}}{\partial p}\right\} - k\frac{\partial}{\partial p}\left\{\overline{U}\left(-k^2 + \frac{\partial^2}{\partial y^2}\right) + \beta - \overline{U}_{yy}\right\}\Psi_i\right] \tag{2.9}$$

$$\frac{\sigma}{f_0}\left(-k^2 + \frac{\partial^2}{\partial y^2}\right)W_i + f_0\frac{\partial^2 W_i}{\partial p^2} = \left[-k\left(-k^2 + \frac{\partial^2}{\partial y^2}\right)\left\{\overline{U}\frac{\partial\Psi_r}{\partial p} - \Psi_r\frac{\partial\overline{U}}{\partial p}\right\} + k\frac{\partial}{\partial p}\left\{\overline{U}\left(-k^2 + \frac{\partial^2}{\partial y^2}\right) + \beta - \overline{U}_{yy}\right\}\Psi_r\right]. \tag{2.10}$$

3. *Numerical integration of the 10-layer quasi-geostrophic model*

A finite difference representation of (2.7) through (2.10) for the model shown schematically in Fig. 4, was integrated using centered differences in space and time. A forward difference in time was used for the first time step and also at every 50th time step, to suppress the separation of the solutions at even and odd numbered time steps. The upper and lower boundary conditions were $\omega' = 0$ at $p = 0$ and $p =$

1000 mb. The lateral boundary conditions were $v' = 0$, i.e., $\psi' = 0$ at the lateral boundaries.

Integrations were performed for two geometrical configurations (Fig. 4). In the first case (domain I), a vertical wall was placed at 28.75N. In the second case (domain II), steeply-sloping Himalayan topography was simulated by a vertical wall extending

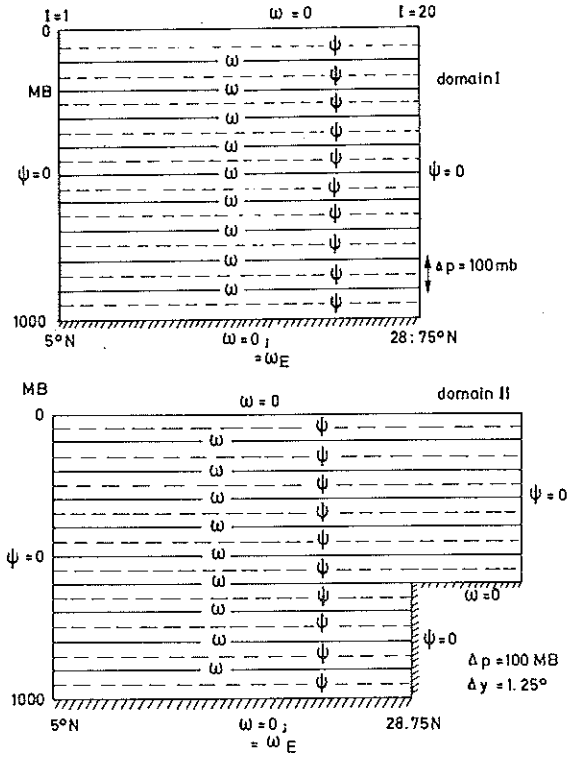

Figure 4
Schematic representation of the ten-layer model for domain I and domain II.

up to 600 mb; the Tibetan plateau extended polewards to 40N, which is the northernmost limit of the domain of integration in the model. A horizontal grid length (Δy) of 138.89 km (1.25 degrees of latitude) and a vertical grid length (Δp) of 100 mb, were used for numerical integrations. The time increments (Δt) used depended upon the wave number $k(=2\pi/L$, where L is the wavelength); the actual values of Δt were given by

$$\Delta t = (k\overline{U}_{\max})^{-1} \quad \text{with} \quad \overline{U}_{\max} = 40 \text{ m/s}.$$

The tendency terms $\partial\Psi_n/\partial t$ and $\partial\Psi_j/\partial t$, were found from (2.7) and (2.8) by use of a one-dimensional relaxation technique. The Liebman relaxation technique with overrelaxation coefficient of 0.3 was used to solve (2.9) and (2.10) at each time step. At the end of every 50 time steps, the phase speed c and growth rate ν were calculated

from (2.5) and (2.6). If they had converged to constant values, the integration was terminated. All the integrations began with a constant value of Ψ specified over the whole domain.

It may be pointed out that KLEIN (1974) used $\Delta y = 300$ km for similar numerical calculations and found that for a middle latitude winter profile of $\bar{U}(y, p)$, the most unstable wavelength was 4000 km. In order to assess the effect of the horizontal grid resolution (Δy), three experiments with $\Delta y = 69.45$ km, 138.9 km and 277.8 km were carried out. For the given $\bar{U}(y, p)$, the wavelength of maximum growth rate remained nearly the same for the cases $\Delta y = 69.45$ km and $\Delta y = 138.9$ km, but for the case $\Delta y = 277.8$ km, the wavelength of maximum growth rate increased by nearly 1000 km. These integrations indicated that coarse resolution may introduce a numerical viscosity which may change the shape of the growth rate curve.

4. Structure of the most unstable mode

Figure 5 shows the growth rate and phase speed versus wavelength curves obtained for domains I and II. In both these cases, the wavelength of the most rapidly growing

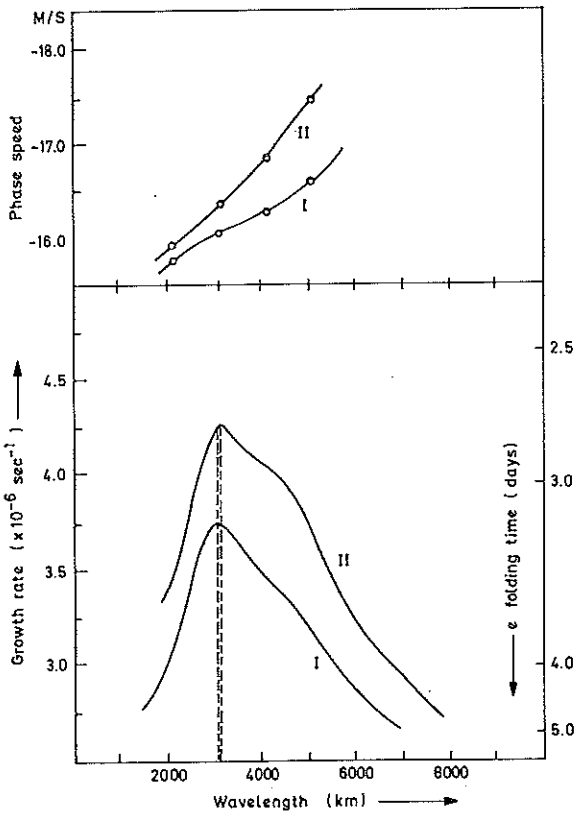

Figure 5
Growth rate and phase speed versus wavelength for domain I and domain II.

perturbation is 3000 km. The *e*-folding times for cases I and II were 3.2 days and 2.6 days, respectively. This difference in the growth rates is due to the differences in available kinetic energy density. These, in turn, are due to the relative locations of the subtropical westerly jet and the tropical easterly jet at 150 mb. Figure 6 shows the structures of the amplitude and phase of Ψ for both cases. The amplitudes are found to be concentrated at 150 mb and fall off very rapidly at the lower layers.

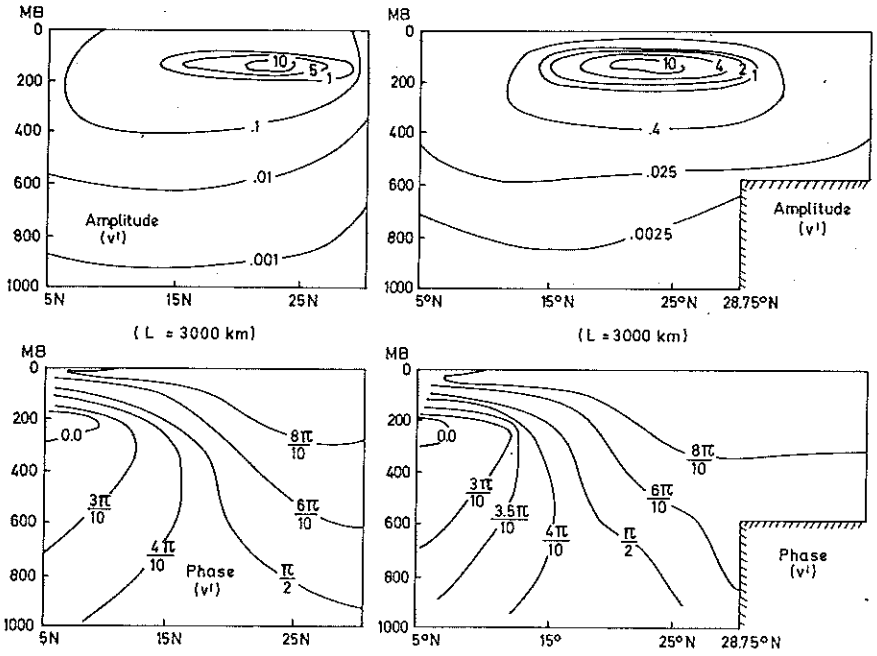

Figure 6
Amplitude and phase structure of the most unstable mode (wavelength = 3000 km) for domain I and domain II.

Since the amplitudes vary over orders of magnitude in the vertical, the phase lines are not very meaningful. The presence of an elevated plateau in domain II has no appreciable effect on the structure of the perturbation above 600 mb. It only affects the kinematics near the plateau boundary.

These results suggest that it is the barotropic instability of the flow at 150 mb which is responsible for the structure and the growth of the most unstable mode; since the model is vertically coupled through the $f_0(\partial\omega/\partial p)$ term, the fastest growing mode of the barotropically unstable 150 mb flow dominates the whole domain. This suggestion will be examined further in the next section.

Since the horizontal scale of the most unstable mode is about 3000 km, the horizontal uniformity of the mean zonal flow over a longitudinal belt of 3000 km was examined by computing the cross-section of potential vorticity along 73E and 100E.

It was found that the mean zonal flow is homogeneous between the longitudes 73E and 100E, and therefore, such a perturbation analysis is justified.

5. *Energetics of the most unstable mode*

In order to gain some further insight into the characteristics of the unstable modes, energy transformations were calculated for the most unstable mode ($L =$ 3000 km) for domains I and II. Results for both domains were nearly identical (the northern boundary did not affect the results), because the amplitudes of the fastest growing perturbations were concentrated at 150 mb.

Expressions for the conversion of eddy kinetic energy to zonal kinetic energy, C(KE, KZ); for zonal available potential energy to eddy available potential energy, C(AZ, AE); and for eddy available potential energy to eddy kinetic energy, C(AE, KE),

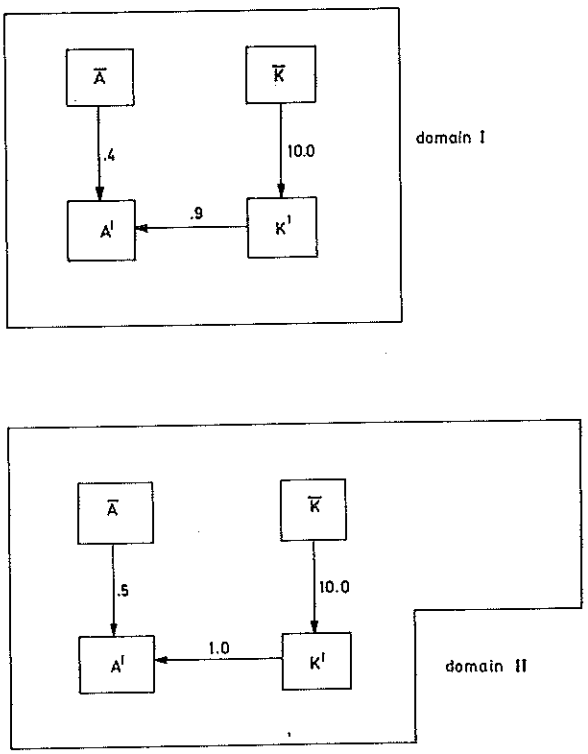

Figure 7
Energy transformations (in arbitrary units) for the most unstable mode (wavelength = 3000 km) for domain I and domain II.

are given as follows:

$$\mathrm{C(KE, KZ)} = \int_0^{p_0}\int_0^{D} \Psi \frac{\partial^2(u'v')}{\partial y^2}\,dy\,dp = \frac{k}{2Dg}\int_0^{p_0}\int_0^{D}\frac{\partial \bar{U}}{\partial p}\left(\Psi_i\frac{\partial \Psi_r}{\partial y} - \Psi_r\frac{\partial \Psi_i}{\partial y}\right)dy\,dp$$

$$\mathrm{C(AZ, AE)} = \int_0^{p_0}\int_0^{D}\frac{f_0^2}{\sigma}\frac{\partial \bar{\Psi}}{\partial y}\frac{\partial}{\partial p}\left\langle\frac{\partial \psi'}{\partial x}\frac{\partial \psi'}{\partial p}\right\rangle dy\,dp$$

$$= \frac{kf_0^2}{2Dg}\int_0^{p_0}\int_0^{D}\frac{1}{\sigma}\frac{\partial \bar{U}}{\partial p}\left(\Psi_r\frac{\partial \Psi_i}{\partial p} - \Psi_i\frac{\partial \Psi_r}{\partial p}\right)dy\,dp$$

$$\mathrm{C(AE, KE)} = \int_0^{p_0}\int_0^{D} f_0\,\omega'\frac{\partial \psi'}{\partial p}\,dy\,dp = \frac{f_0}{2Dg}\int_0^{p_0}\int_0^{D}\left(W_r\frac{\partial \Psi_r}{\partial p} + W_i\frac{\partial \Psi_i}{\partial p}\right)dy\,dp$$

where D = lateral width of the domain = $19\Delta y$ and p_0 = surface pressure = 1000 mb, $\langle\ \rangle$ denotes domain average.

Figure 7 shows the numerical values of these conversions in arbitrary units.

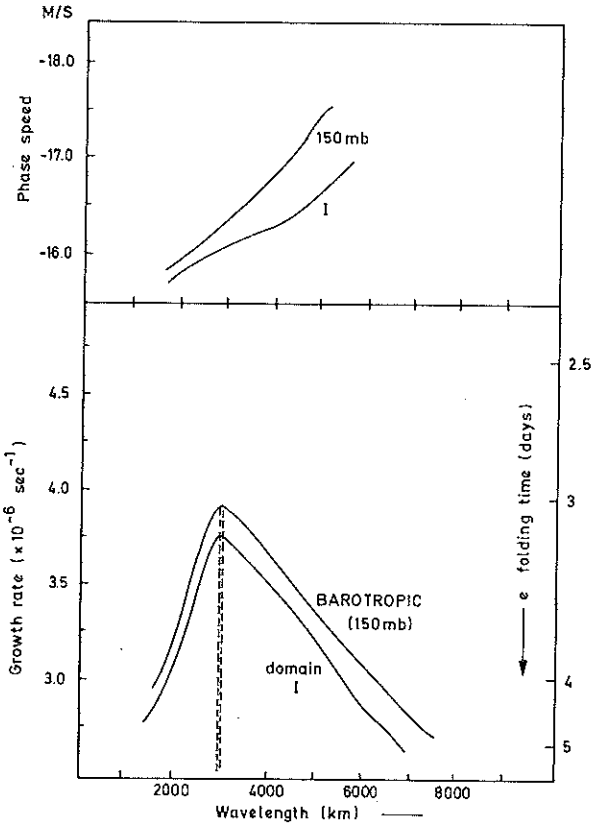

Figure 8
Growth rate and phase speed versus wavelength for domain I and for barotropic instability at 150 mb.

We see that the most dominant conversion is from KZ to KE, which demonstrates the importance of barotropic instability.

This also suggests that the barotropic instability of the zonal flow at 150 mb may be the primary excitation mechanism for these modes. In order to verify this result, a barotropic instability analysis was performed for the zonal flow at the 150 mb level.

Figure 8 displays the results of the barotropic-baroclimic instability analysis for the entire domain I, and the barotropic instability analysis of the zonal flow at 150 mb. It may be seen that both curves are almost identical, confirming the earlier suggestion that most of the contribution to the instability shown in Fig. 5 comes from the barotropic instability at 150 mb. In fact, the growth rate is slightly higher for the barotropic (150 mb) case, because the lower levels have weaker horizontal and vertical shears, and therefore, smaller available kinetic energy and available potential energy. The same conclusion could have been reached by examining the time evolution of the patterns of convergence for phase speed and growth rate during the integration. For example, it was observed that the convergence of c and ν occurred first at 150 mb and then proceeded downwards. This reflects the influence of the instability at 150 mb level on the lower levels, through the vertical coupling. However, the time scale over which all the levels become 'contaminated' by the instability of 150 mb is very large (50 days), compared to the period of the most unstable wave at 150 mb (3 days).

The growth rates and the phase speeds for a range of wavelengths were also calculated for the case where $\partial U/\partial p = 0$ and $U(y)$ at each level was the same as $U(y)$ at 150 mb. The results were very similar to the one shown in Fig. 8 for the 150 mb barotropic case.

6. *Concluding remarks*

It is found that the meridional profile of the zonal wind at 150 mb is barotropically unstable and that the fastest growing mode has the wavelength of 3000 km. The structure of the most unstable mode is such that most of the amplitude is concentrated at 150 mb. The conversion C(AZ, AE) is small and, therefore, the baroclinic instability mechanism is not important.

In an earlier paper COLTON (1973) has suggested that 'nonlinear barotropic interaction between the quasi-stationary forced planetary waves and transient synoptic scale waves is important in producing several features of the tropical upper tropospheric general circulation. In particular, the development of the small-scale waves and vortices often present in the mid-oceanic troughs and the disturbances observed by Krishnamurti which form along the easterly jet over the Indian Ocean is shown to be due to scale interactions involving short-term nonlinear barotropic instability.'

In the present paper we have used the linear barotropic instability analysis to

show that the mechanism for the generation of transient synoptic scale waves is the barotropic instability of the mean zonal flow. The phase speed of the computed most unstable perturbation agrees reasonable well with the observed phase speed of 10–12° longitude/day at 200 mb (KRISHNAMURTI, 1971). Since barotropically unstable perturbations draw energy from the mean motion, these results are also in agreement with the hypothesis of COLTON (1973) that small-scale waves at 200 mb are continuously draining the energy of the mean motion and quasi-stationary large-scale waves.

Finally it may be remarked that it is rather unlikely that the barotropically unstable disturbances at 150 mb could account for the observed monsoon depressions which have their amplitude maxima at the lower tropospheric levels and are rarely detected at 200 mb. Therefore, proper inclusion of moist-convective heating seems to be not only desirable, but essential to explain the growth of the monsoon depressions. The author (SHUKLA, 1976) has investigated the instability of a basic state in which the zonal wind has horizontal and vertical shear, the vertical thermal structure is conditionally unstable, and the moist convective heating is parameterized in terms of the large-scale variables. These results have been reported in another paper (SHUKLA, 1977).

Acknowledgements

The author expresses his gratitude to Professors Jule G. Charney and Norman A. Phillips, who were the thesis advisers at MIT, for their valuable suggestions and guidance. Computer facility at the Goddard Institute of Space Studies was used for performing the numerical integrations.

REFERENCES

CHARNEY, J. G. and STERN, M. E. (1962), *On the stability of internal baroclinic jets in a rotating atmosphere*, J. Atmos. Sci. *19*, 159–172.

COLTON, D. E. (1973), *Barotropic scale interactions in the tropical upper troposphere during the northern summer*, J. Atmos. Sci. *30*, 1287–1302.

KLEIN, W. D. (1974), *Ozone kinematics and transports in unstable waves*, PhD Thesis, Dept. of Meteorology, MIT, Cambridge, Mass.

KRISHNAMURTI, T. N. (1971), *Observational study of the tropical upper tropospheric motion field during the northern hemisphere summer*, J. Appl. Meteor. *10*, 1066–1096.

KRISHNAMURTI, T. N., KANAMITSU, M., GODBOLE, R. CHANG, C. B., CARR, F. and CHOW, J. H. (1976), *Study of a monsoon depression (II), Dynamical structure*, J. Meteor. Soc. Japan *54*, 208–255.

SHUKLA, J. (1976), *On the dynamics of Monsoon depressions*, ScD Thesis, Dept. of Meteorology, MIT, Cambridge, Mass.

SHUKLA, J. (1977), *CISK-barotropic-baroclinic instability and the growth of monsoon depressions*, Submitted to J. Atmos. Sci. for publication.

(Received 15th June 1977)